Published in final edited form as:
Opt Express. 2009 March 2; 17(5): 3619–3629.

Miniature swept source for point of care Optical Frequency Domain Imaging

Brian D. Goldberg[1,2], **S.M. Reza Motaghian Nezam**[1], **Priyanka Jillella**[1], **Brett E. Bouma**[1,2], and **Guillermo J. Tearney**[1,*]

1*Harvard Medical School and the Wellman Center for Photomedicine, Massachusetts General Hospital, 50 Blossom St., Boston, MA 02114*

2*Harvard-MIT Division of Health Sciences and Technology, 77 Massachusetts Avenue, E25-119, Cambridge, MA 02139*

Abstract

Point of care (POC) medical technologies require portable, small, robust instrumentation for practical implementation. In their current embodiment, optical frequency domain imaging (OFDI) systems employ large form-factor wavelength-swept lasers, making them impractical in the POC environment. Here, we describe a first step toward a POC OFDI system by demonstrating a miniaturized swept-wavelength source. The laser is based on a tunable optical filter using a reflection grating and a miniature resonant scanning mirror. The laser achieves 75 nm of bandwidth centered at 1340 nm, a 0.24 nm instantaneous line width, a 15.3 kHz repetition rate with 12 mW peak output power, and a 30.4 kHz A-line rate when utilizing forward and backward sweeps. The entire laser system is approximately the size of a deck of cards and can operate on battery power for at least one hour.

1. Introduction

Point-of-care (POC) technologies aim to bring advances in medical technology directly to the patient. A successful POC technology must be small, inexpensive, lightweight, accurate, robust, and easy to use. POC testing, imaging and diagnostics are becoming more and more common within many medical settings including primary, home, and emergency care[1].

Imaging technologies have the potential to play a key role within the field of new POC technologies, allowing the physician to see deeper, with higher resolution, and with greater contrast than with the naked eye. At the point of care, imaging can provide crucial diagnostic information[2], guide procedures[3,4], and identify tumor margins during surgery [5]. In other settings, new imaging technologies are performing comprehensive screening in ways that may eliminate the need for biopsies altogether[6–8].

One example where optical POC technologies can make a difference is in the setting of Fine Needle Aspiration biopsy (FNAB). FNAB is often the first line of diagnosis for a palpable mass in the breast and thyroid[9–11]. In order to perform an FNAB, the mass is manually stabilized, a small diameter needle (typically 23–25 gauge) is inserted into the mass, and a small amount of tissue or fluid is aspirated into the needle. The aspirate within the bore of the needle is then expressed onto a slide, smeared, stained, and examined by a pathologist. Due to

**Corresponding author:* E-mail: gtearney@partners.org.

the small size of the needle, patient discomfort is generally limited to the initial stick of the needle. Manual palpation of a superficial mass is often the only cue for determining the optimal position of the needle in tissue during biopsy. As a result, when not guided by an imaging modality, breast FNAB's obtain diagnostic tissue in approximately 65–78% of cases.[12–14]. Recently, groups have investigated the use of optical technologies for guiding FNAB's and other needle based biopsy techniques with high sensitivity and specificity[4,5,15–20].

Optical frequency domain imaging (OFDI)[15], also known as swept-source OCT[21,22], is a high-resolution (~10 μm), cross-sectional, fiber-optic imaging method that is capable of measuring tissue microstructure, birefringence (correlated to collagen that may be found in blood vessel adventitia)[23,24], and blood flow (Doppler)[14,25]. OFDI systems are comprised of three main elements; 1) A rapidly swept laser, 2) a fiber-based interferometer and 3) detection and processing electronics. A portable OFDI system requires miniature components for all three elements. In this paper we will focus on the miniature wavelength-swept laser.

The development of high-speed wavelength-swept lasers for OFDI has advanced at a rapid pace. There are several commonly applied designs for these sources. One common design uses a semiconductor gain medium within a unidirectional fiber ring cavity and an intracavity or extended cavity swept wavelength filter. Swept wavelength filters can be comprised of a diffraction grating and polygon mirror[26], galvanometer scanning mirror[27], or scanning Fabry-Perot filters[22,28]. Other designs allow all wavelengths to propagate within the cavity and control the round-trip such that a single wavelength returns to the tuning filter at harmonics of the round trip time. These designs are known as Fourier Domain Modelocked Lasers (FDML) and can achieve very high sweep rates in excess of 300 kHz[29]. Linear cavity laser designs have also been employed where wavelength-tuning is achieved by diffraction grating/reflecting mirror combinations[30–33]. Linear cavities often provide a bidirectional wavelength sweep where differences in forward and backward sweep dynamics are determined by cavity length and tuning speed[34]. Common to all designs, however, is a prohibitively large form-factor for POC deployment.

In this paper we present a high-speed, high-power, miniature wavelength swept laser for use in point-of-care OFDI applications. The laser utilizes a linear cavity design and can achieve 12 mW of peak output power, a 75 nm tuning bandwidth, and 0.24 nm instantaneous line width. The laser has a bidirectional sweep rate of 15.3 kHz enabling 30.6 kHz OFDI A-line generation. In addition, the entire laser can be operated on battery power and packaged in a form factor that's roughly the size of a deck of cards.

2. Experimental setup

2.1. Laser Design

Figure 1 shows the source design based on a tunable optical filter using a reflection grating and a miniature resonant scanning mirror. The gain element of the laser was a single angle facet (SAF) gain module (Covega, Inc. SAF 1136), in which the waveguide was terminated at one end by a normal-incidence facet at 90% reflection, forming an output coupler, and at the second end by an angled facet at 0.01% reflection, which delivered light to an external cavity [35]. Wavelength selection was accomplished using a 1200 l/mm diffraction grating, oriented to an angle of incidence of approximately 80 degrees, followed by a resonant scanning galvanometer mirror (Electro-Optical Products Corp. SC-30) and a fixed mirror. The external cavity was approximately 8 cm.

Light from the gain medium was dispersed by the grating according to the familiar grating equation $\lambda = p(\sin\alpha + \sin\beta)$, where λ is the incident wavelength, p the grating pitch, and α and

β the incident and diffracted angles respectively. The FWHM bandwidth of the filter is determined by the grating pitch, incident angle, and beam diameter and given by $(\delta\lambda)_{FWHM} / \lambda_0 = (4 \ln 2)^{½}/\pi*(p/m)\cos \alpha/w$ where *m* is the diffraction order, and W is the 1/e^2 width of the Gaussian beam[26]. The beam width was approximately 0.5 mm corresponding to a $(\delta\lambda)_{FWHM}$ of 0.21 nm.

The tuning bandwidth of the filter is given by $\Delta\lambda = p \cos(\beta_0)\Delta\beta$, where Δβ is the physical scan angle of the resonant scanner and β_0 is the output angle at the center wavelength. It should be noted that resonant scanner scan angles are sometimes reported as optical scan angle which is equal to double the physical scan angle of the mirror. In this paper, we refer to Δβ as the physical scan angle. Resonant scanners have scan angles that decrease with increasing frequency. At 15.3 kHz, the scan angle was only ~3 degrees. Therefore the resonant scanner was further deflected onto a fixed mirror to work in the so called "2X" configuration and double the filter's effective scan angle. Similar configurations have been used to increase the FSR by using multiple mirror reflections[36,37]. At 6 degrees total optical deflection, the tuning bandwidth was 69.1 nm which makes the theoretical finesse 329.

Even though the gain bandwidth is broader than the filter free spectral range and the filter tuning range lies within the gain bandwidth, the duty cycle of the laser is further limited by the physical size of the resonant and fixed mirrors as well as their distance from the diffraction grating. In order to utilize the entire scan angle of the resonant scanner, the resonant scanner must be placed close enough to the diffraction grating to avoid clipping of the optical beam at the edge of the resonant scanning mirror. It can be shown that the distance restriction for the 2X configuration is given by $r < d / \tan(\Delta\beta) 2W \cos \beta_0 / \cos \alpha$. Here, *d* is the physical size of the resonant mirror (4 mm) and r is the distance from the grating to the resonant mirror. A similar expression can be derived for the distance between the resonant and fixed mirrors. If these restrictions are met, and the tuning bandwidth is entirely within the gain-bandwidth of the gain medium, the laser will have 100% duty cycle. Otherwise, if the scan angle is increased such that the tuning bandwidth is outside the gain bandwidth or the beam is clipped, the duty cycle will be less than 100%. Currently, the resonant mirror size cannot be increased without decreasing the resonant scan frequency.

The resonant mirror was driven with a high-Q resonant electric drive circuit (Electro-Optical Products Corp., ED-M) that required very low electrical power. It can be operated for long periods of time with a 9V battery. The laser source was driven with commercially available miniature laser (Wavelength Electronics FL500) and temperature (Wavelength Electronics WTC 3243 HB) controllers and powered by 3V lithium batteries. The entire laser, including optics and electronics was configured with a form factor that is approximately the size of a deck of cards (Fig. 1). The actual physical size of the laser optics was 3 in. × 2.5 in. × 3 in.

2.2. OFDI imaging setup

The OFDI imaging setup is shown in Fig. 2. The laser output was directed through an 80/20 splitter into sample and reference arms. Each arm consisted of a circulator and signal reflection elements. During calibration and testing, a fixed reflector was placed in both the reference and sample arms. During imaging, the sample arm consisted of an X-Y galvanometer scanner (Cambridge Technology 6220H), and a 30 mm focal length lens. The reference arm contained a neutral density attenuator to control the power on the detector. The signals were recombined through a 50/50 splitter and directed input into an 80 MHz balanced receiver (New Focus 1817). The signal was digitized at 50 MS/s with a 14-bit DAQ (Gage: CompuScope 14200). The A/D acquisition was triggered directly from the TTL output of the resonant scanner driver. Samples were re-interpolated to equal spacing in K-space[15].

3. Results

3.1 Laser characteristics

A characteristic laser output trace is shown in Fig. 3. The peak output power was ~12 mW (6.0 mW average power) with only subtle power differences between the forward and backward wavelength sweeps. The green trace is the TTL signal from the resonant driver. The resonant frequency was measured to be 15.3 kHz. The transition from forward to backward sweep direction occurred within the gain bandwidth of the SAF, resulting in continuous lasing during this transition. During this transition, the speed of the resonant scanner eventually slows to zero and a highly non-linear scanner motion occurs. The plateau and dip may be a mismatch between the linear sampling of the detection electronics and the non-linear motion of the resonant scanner. The cavity mode spacing was 1.9 GHz which may have contributed to the high-frequency noise seen in the laser trace. The overall duty cycle was 87.6%. The laser produced an edge to edge tuning range of 75 nm (Fig. 4) centered at 1340 nm. The image was taken by applying the max-hold function on the optical spectrum analyzer (OSA) (HP 70950B) at 0.2 nm resolution to avoid mismatch between the laser sweep rate and the OSA sampling rate. The sharp peaks at short wavelengths in the scan are a result of the sinusoidal scan pattern resulting in increased time spent at the edges. The increased tuning range compared with the theoretical result is attributed to slightly larger scan angle of the resonant scanner.

After splitting the light into sample and reference arms and accounting for any interferometer losses, there was 4.2 mW of average power at the sample. A variable neutral density filter was adjusted such that 18 μW of power returned to each detector from the reference arms. The total sample arm power returning to the detectors from a fixed reflector was 2.5 mW. The fringe pattern from a fixed reflector is shown in Fig. 5.

The sensitivity and ranging depth were measured with a 43.5 dB attenuator in the sample arm path. The result from a fixed reflector at 500 μm for both forward and backward wavelength sweeps is shown in Fig. 6. The maximum sensitivity measured at zero delay was 98.1 dB. The dynamic range for the sensitivity measurement was 54.6 dB. The theoretical sensitivity including all noise sources was 100.3 dB with a shot noise limited sensitivity of 116.1 dB. The difference results from incomplete RIN noise suppression and thermal noise which were dominant over shot noise at the operating conditions. Figure 7 shows the SNR drop-off as a function of depth. The ranging depth as measured by the 6 dB drop in SNR was ~1.75 mm, indicative of an instantaneous linewidth of 0.24 nm, approximately 13% broader than predicted (0.21 nm). We attribute this to sub-optimal collimation from the SAF which decreases the effective beam size as well as errors from the interpolation into K-space which affect the 6 dB roll off calculation.

3.2 Battery powered operation

We have tested the battery-powered operation for over an hour with only minimal drop in output power (Fig. 8). This operating duration may be sufficient for point-of-care deployment in which a 10–15 minute operation is anticipated followed by recharging time between applications.[38]

3.3 OFDI Imaging

Images obtained from the ventral surface of a human finger are shown in Fig. 9. The image is a 5 mm transverse sweep with 300 A-lines per frame, shown at 8-bit resolution. Images from the forward, backward, and combined (average of forward and backward) wavelength sweeps are presented. There were negligible differences between the forward and backward sweep images. This enables imaging at the full 30.6 kHz rate provided by the source, which can be employed to reduce speckle noise as shown in the combined image.

4. Discussion

A truly point-of-care OFDI system requires a small, portable, and fully packaged swept laser, interferometer, and detection, processing, and display electronics. We have focused only on the laser portion in this paper and shown the capability of a miniature, battery-powered laser for producing high quality OFDI images. There remain a number of limitations and challenges towards implementing this design in a clinical POC system. First, although the laser optics are only the size of a deck of cards, the drive electronics require additional space. Together, the commercially available laser driver, temperature controller, and resonant scanner drivers would fit into a package roughly the size of 2–3 decks of cards including the batteries that drive each component. A fully custom built drive circuit could incorporate all the drivers onto a single printed circuit board to minimize the electronic foot print. Similarly a custom battery cell and appropriate voltage regulators could be used to replace the three separate batteries we used in this study. Moreover, a fully packaged source may require additional temperature cooling to keep the laser output stable. The resonant scanner design also provides challenges for making the laser hand-held. Movement and vibrations can disrupt the resonant scanning mechanism. The resonant scanner used in this study has a counterweight that's used to achieve high scan speeds and improve stability. We have picked up the laser system and observed only small fluctuations in the SNR from a fixed reflector. This has not been tested in a systematic way and we expect that further work will be needed to design the packaging to ensure the resonant scanner is highly stable.

The overall laser performance is determined by the filter efficiency and the drive current within the gain medium which sets the cavity gain. There is an inherent tradeoff between grating efficiency and filter linewidth. In order to achieve a sufficiently narrow linewidth required an incident angle of ~80° which is well away from the blaze angle of 36.5°. This can be improved by using a SAF with a larger beam diameter, allowing a shallower incident angle onto the grating for the same resolution. In addition, the gain medium current was limited to 500 mA which is the maximum current the miniature laser driver can achieve. A driver that can provide more drive current should improve the output power and improve the system sensitivity. However, increased drive current requires more battery power which would reduce the operating time of the laser system. The small scan angle of the resonant scanner limits the tuning bandwidth. Larger scan angles can be achieved by reducing the resonant frequency.

The interferometer and detection electronics also need to be miniaturized for a POC OFDI system and the components used in this study are not suitable for fully portable use. One solution would be to use a common path interferometer that only requires a single circulator attached to the imaging probe. Common-path approaches have additional challenges such as setting the reference light appropriately to achieve good SNR and an inability to work in dual-balanced mode. Similarly, the imaging optics used in this study are large and have high power consumption. In this study they were only used to demonstrate the imaging capabilities of the laser and a portable imaging system would require distal optics such as MEMS based scanners to generate an image.

A truly portable, battery powered source and OFDI system are not necessary for every POC application. Many clinical settings have access to power outlets and sufficient space to accommodate a cart based device. However, a fully portable OFDI system, including this laser design, would allow OFDI systems to be used in a broader range of clinical applications including ambulatory emergency medical services as well as battlefield medicine and in the austere settings of developing countries.

5. Conclusion

We have built a novel miniature wavelength-swept laser suitable for point-of-care OFDI. The system can be fully battery powered, has a small footprint, and achieves a peak output power of 12 mW, 75 nm tuning bandwidth, and 0.24 nm instantaneous linewidth. Wavelength tuning is accomplished by using a reflection grating and a miniature resonant scanning mirror rotating at 15.3 kHz. Utilizing both forward and backward wavelength sweeps enables OFDI imaging at 30 kHz A-line rates. Images of the ventral surface of a human finger were obtained with good imaging depth and sensitivity. Future work will focus on the integration of this laser with a system for guiding needle placement in the biopsy, trauma care, and other POC clinical settings.

References and links

1. Price CP, Kricka LJ. Improving Healthcare Accessibility through Point-of-Care Technologies. Clin. Chem 2007;53:1665–1675. [PubMed: 17660275]
2. Beaulieu Y. Bedside echocardiography in the assessment of the critically ill. Crit. Care. Med 2007;35:S235–S249. [PubMed: 17446784]
3. Gupta S, Madoff D. Image-guided percutaneous needle biopsy in cancer diagnosis and staging. Tech. Vasc. Interv. Radiol 2007;10:88–101. [PubMed: 18070687]
4. Goldberg BD, Iftimia NV, Bressner JE, Pitman MB, Halpern E, Bouma BE, Tearney GJ. An automated algorithm for differentiation of human breast tissue using low coherence interferometry for fine needle aspiration breast biopsy. J. Biomed. Opt 2008;13:014014. [PubMed: 18315372]
5. Zysk AM, Boppart SA. Computational methods for analysis of human breast tumor tissue in optical coherence tomography images. J. Biomed. Opt 2006;11
6. Hsiung P-L, Pantanowitz L, Aguirre AD, Chen Y, Phatak D, Ko TH, Bourquin S, Schnitt SJ, Raza S, Connolly JL, Mashimo H, Fujimoto JG. Ultrahigh-resolution and 3-dimensional optical coherence tomography ex vivo imaging of the large and small intestines. Gastrointestinal Endoscopy 2005;62:561–574. [PubMed: 16185971]
7. Yun SH, Tearney GJ, Vakoc BJ, Shishkov M, Oh WY, Desjardins AE, Suter MJ, Chan RC, Evans JA, Jang I-K, Nishioka NS, de Boer JF, Bouma BE. Comprehensive volumetric optical microscopy in vivo. Nat. Med 2007;12:1429–1433. [PubMed: 17115049]
8. Westphal V, Rollins AM, Willis J, Sivak MV Jr, Izatt JA. Correlation of endoscopic optical coherence tomography with histology in the lower-GI tract. Gastrointestinal Endoscopy 2005;61:537–546. [PubMed: 15812406]
9. Frable MAS, Frable WJ. Fine-Needle Aspiration Biopsy of Salivary-Glands. Laryngoscope 1991;101:245–249. [PubMed: 2000011]
10. Mandreker SRS, Nadkarni NS, Pinto RGW, Menezes S. Role of Fine-Needle Aspiration Cytology as the Initial Modality in the Investigation of Thyroid Lesions. Acta. Cytologica 1995;39:898–904. [PubMed: 7571967]
11. Klein S. Evaluation of Palpable Breast Masses. American Family Physician 2005;71:1731–1738. [PubMed: 15887452]
12. Scott Boerner NS. Specimen adequacy and false-negative diagnosis rate in fine-needle aspirates of palpable breast masses. Cancer Cytopathology 1998;84:344–348. [PubMed: 9915135]
13. Hindle WH, Chen EC. Accuracy of mammographic appearances after breast fine-needle aspiration. American Journal of Obstetrics and Gynecology 1997;176:1286–1290. [PubMed: 9215186]
14. Zhao Y, Chen Z, Saxer C, Xiang S, de Boer JF, Nelson JS. Phase-resolved optical coherence tomography and optical Doppler tomography for imaging blood flow in human skin with fast scanning speed and high velocity sensitivity. Opt. Lett 2000;25:114–116. [PubMed: 18059800]
15. Yun SH, Tearney GJ, de Boer JF, Iftimia N, Bouma BE. High-speed optical frequency-domain imaging. Opt. Express 2003;11:2953–2963. [PubMed: 19471415]
16. Zysk AM, Adie SG, Armstrong JJ, Leight MS, Paduch A, Sampson DD, Nguyne FT, Boppart SA. Needle-based refractive index measurement using low-coherence interferometry. Opt. Lett 2007;32

17. Li X, Chudoba C, Ko T, Pitris C, Fujimoto JG. Imaging needle for optical coherence tomography. Opt. Lett 2000;25:1520–1522. [PubMed: 18066265]
18. Johns M, Giller CA, German D, Liu H. Determination of reduced scattering coefficient of biological tissue from a needle-like probe. Opt. Express 2005;13:4828–4842. [PubMed: 19498468]
19. Zhu YZ, Wang AB. Miniature fiber-optic pressure sensor. IEEE Photon. Technol. Lett 2005;17:447–449.
20. Reed WA, Yan MF, Schnitzer MJ. Gradient-index fiber-optics microprobes for minimally invasive in vivo low-coherence interferometry. Opt. Lett 2002;27:1794–1796. [PubMed: 18033366]
21. Choma M, Sarunic M, Yang C, Izatt J. Sensitivity advantage of swept source and Fourier domain optical coherence tomography. Opt. Express 2003;11:2183–2189. [PubMed: 19466106]
22. Huber R, Wojtkowski M, Fujimoto JG. Fourier Domain Mode Locking (FDML): A new laser operating regime and applications for optical coherence tomography. Opt. Express 2006;14:3225–3237. [PubMed: 19516464]
23. de Boer JF, Srinivas SM, Park BH, Pham TH, Chen ZP, Milner TE, Nelson JS. Polarization effects in optical coherence tomography of various biological tissues. IEEE J. Sel. Top. Quantum Electron 1999;5:1200–1204.
24. Oh WY, Yun SH, Vakoc BJ, Shishkov M, Desjardins AE, Park BH, de Boer JF, Tearney GJ, Bouma BE. High-speed polarization sensitive optical frequency domain imaging with frequency multiplexing. Opt. Express 2008;16:1096–1103. [PubMed: 18542183]
25. Vakoc B, Yun S, de Boer J, Tearney G, Bouma B. Phase-resolved optical frequency domain imaging. Opt. Express 2005;13:5483–5493. [PubMed: 19498543]
26. Yun SH, Boudoux C, Tearney GJ, Bouma BE. High-speed wavelength-swept semiconductor laser with a polygon-scanner-based wavelength filter. Opt. Lett 2003;28:1981–1983. [PubMed: 14587796]
27. Yun SH, Boudoux C, Pierce MC, Boer JFd, Tearney GJ, Bouma BE. Extended-cavity semiconductor wavelength-swept laser for biomedical imaging. IEEE Photon. Technol. Lett 2004;16:293–295.
28. Choma M, Hsu K, Izatt J. Swept source optical coherence tomography using an all-fiber 1300-nm ring laser source. J. Biomed. Opt 2005;10:044009.
29. Tumlinson AR, Barton JK, Povazay B, Sattman H, Unterhuber A, Leitgeb RA, Drexler W. Endoscope-tip interferometer for ultrahigh resolution frequency domain optical coherence tomography in mouse colon. Opt. Express 2006;14:1879–1887.
30. Chinn SR, Swanson EA, Fujimoto JG. Optical coherence tomography using a frequency-tunable optical source. Opt. Lett 1997;22:340–342. [PubMed: 18183195]
31. Changho C, Morosawa A, Sakai T. High-Speed Wavelength-Swept Laser Source With High-Linearity Sweep for Optical Coherence Tomography. IEEE J. Sel. Top. Quantum Electron 2008;14:235–242.
32. Lee SW, Kim CS, Kim BM. External Line-Cavity Wavelength-Swept Source at 850 nm for Optical Coherence Tomography. IEEE Photon. Technol. Lett 2007;19:176–178.
33. Huber R, Wojtkowski M, Fujimoto JG, Jiang JY, Cable AE. Three-dimensional and C-mode OCT imaging with a compact, frequency swept laser source at 1300 nm. Opt. Express 2005;13:10523–10538. [PubMed: 19503267]
34. Huber R, Wojtkowski M, Taira K, Fujimoto J, Hsu K. Amplified, frequency swept lasers for frequency domain reflectometry and OCT imaging: design and scaling principles. Opt. Express 2005;13:3513–3528. [PubMed: 19495256]
35. Oh WY, Yun SH, Vakoc BJ, Tearney GJ, Bouma BE. Ultrahigh-speed optical frequency domain imaging and application to laser ablation monitoring. Appl. Phys. Lett 2006;88:103902–103903.
36. Motaghian Nezam SMR. High-speed polygon-scanner-based wavelength-swept laser source in the telescope-less configurations with application in optical coherence tomography. Opt. Lett 2008;33:1741–1743. [PubMed: 18670522]
37. Oh WY, Yun SH, Tearney GJ, Bouma BE. 115 kHz tuning repitition rate ultrahigh-speed wavelength-swept semiconductor laser. Opt. Lett 2005;30:3159–3161. [PubMed: 16350273]
38. Pitman, MB. personal communication. 2007.

Acknowledgements

Funding for this work was provided by the Medical Free Electron Laser Program (FA9550-04-1-0079), Physical Sciences Inc. (NIH 1 R43 CA114896-01), the NIH (1 F31 EB005141–01), and Terumo Corporation. The authors would also like to thank Ben Vakoc and William Oh for their guidance in OFDI imaging and swept-source laser design. Currently SM Reza Motaghianezam is with the Department of Biology, California Institute of Technology, 1200 East California Boulevard, Pasadena, California 91125.

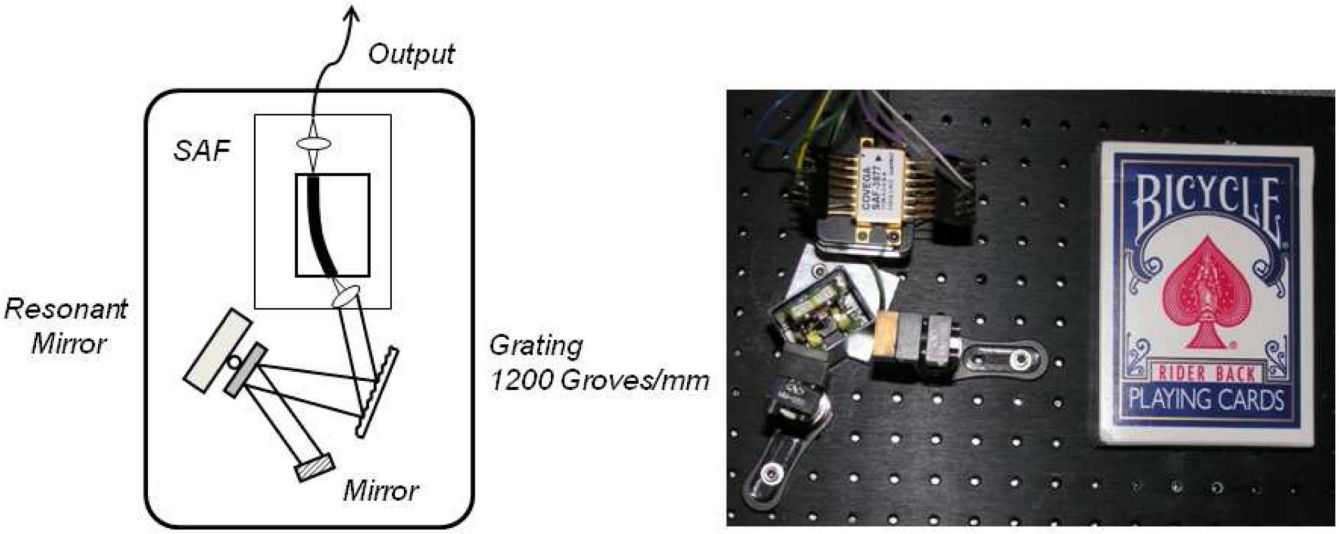

Fig. 1.

Miniature wavelength-swept laser source schematic (left). The output from a semiconductor gain medium illuminated a grating and was deflected via a resonant scanning mirror such that only one wavelength of light was amplified within the laser cavity. As the resonant mirror rotated, the laser's output wavelength was swept in time. A photograph of the source (right) is shown adjacent to a pack of cards for scale.

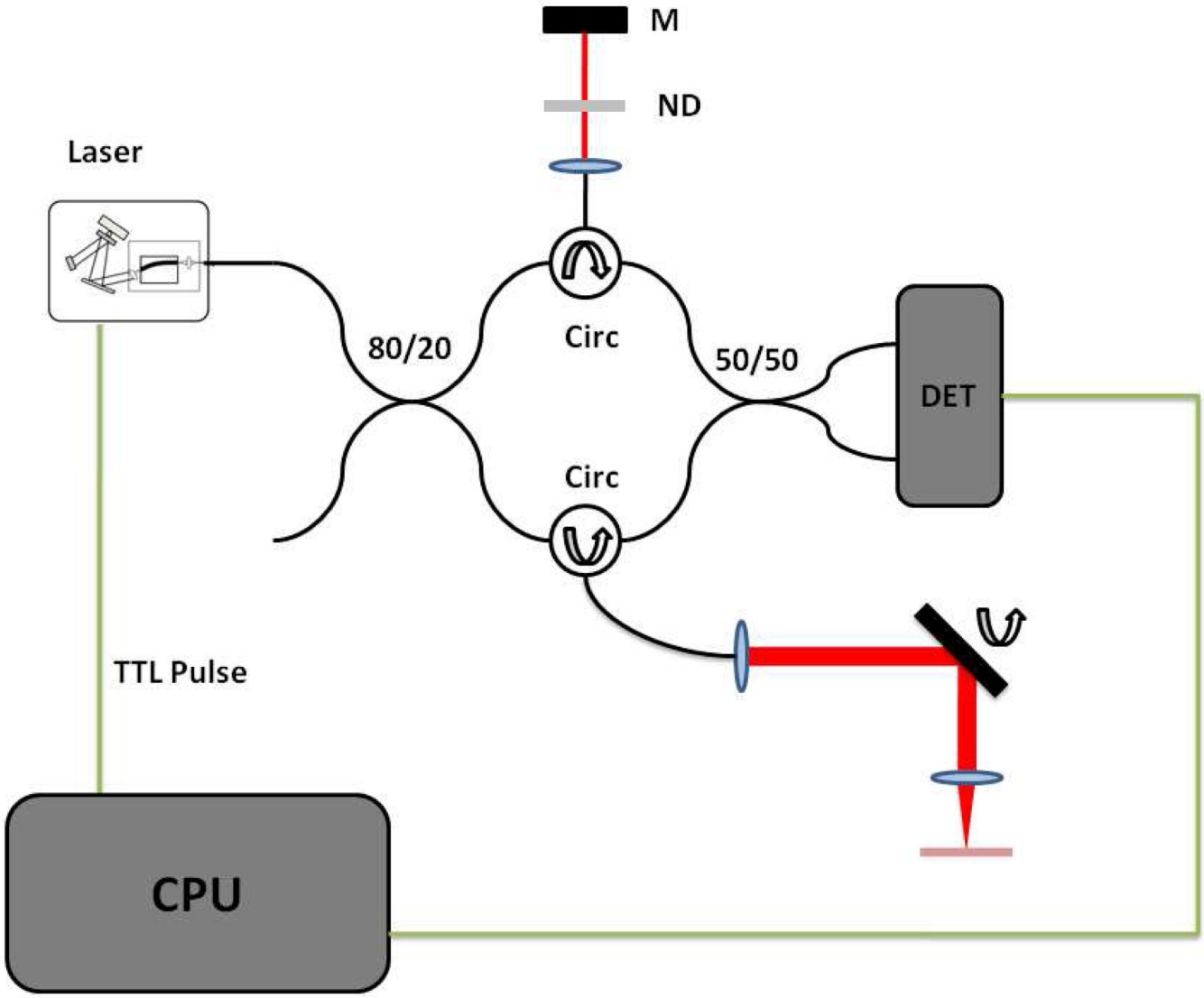

Fig. 2.

OFDI Imaging setup. The output from the swept laser is directed through an 80/20 splitter into reference and sample arms. Each arm contains a circulator and signal reflection elements. The reference arm consists of a neutral density filter and a fixed mirror (M). The sample arm contains a two-axis galvanometer scanning system. The dual balanced detector (DET) output into a computer (CPU) for digitization and processing. The resonant scanner TTL pulse is used for acquisition triggering.

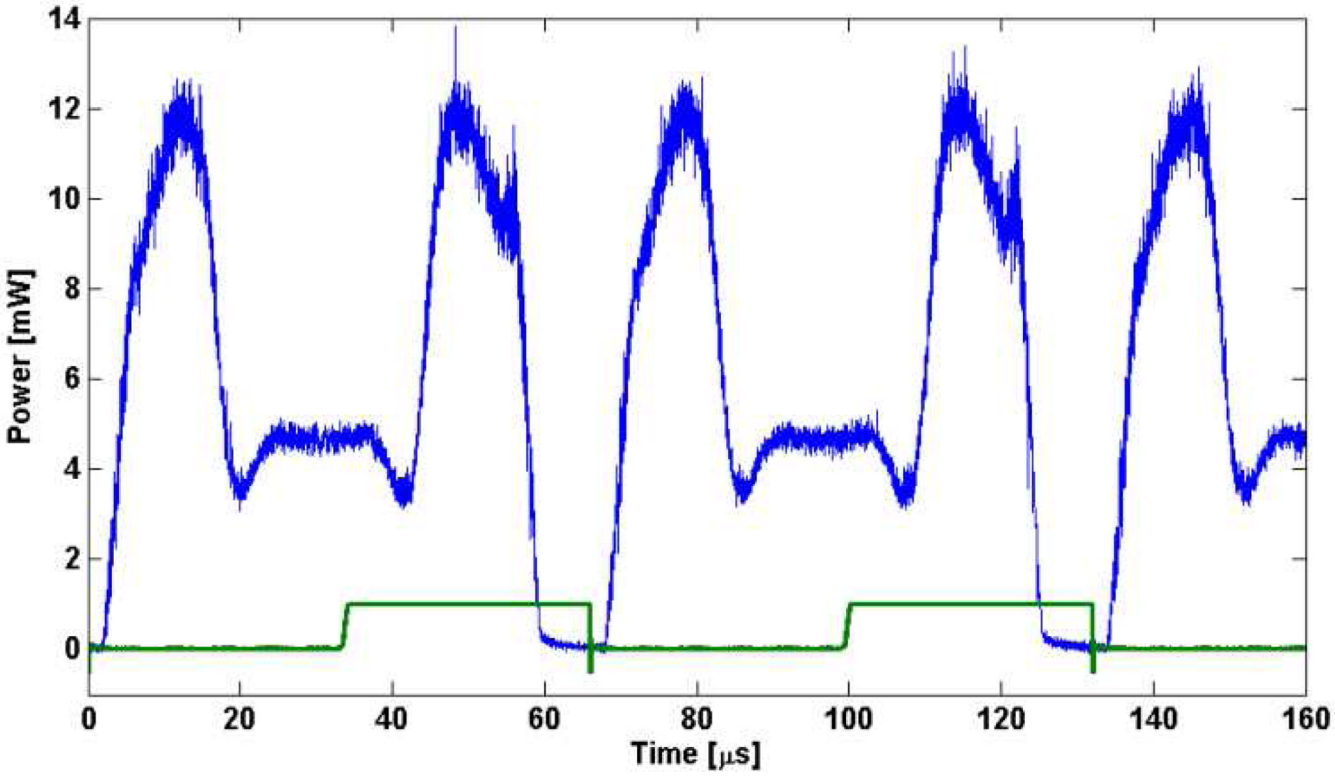

Fig. 3.
Laser trace showing ~2.5 full sweeps of the resonant scanner. Green trace is the TTL output from the resonant scanner and used as the system trigger.

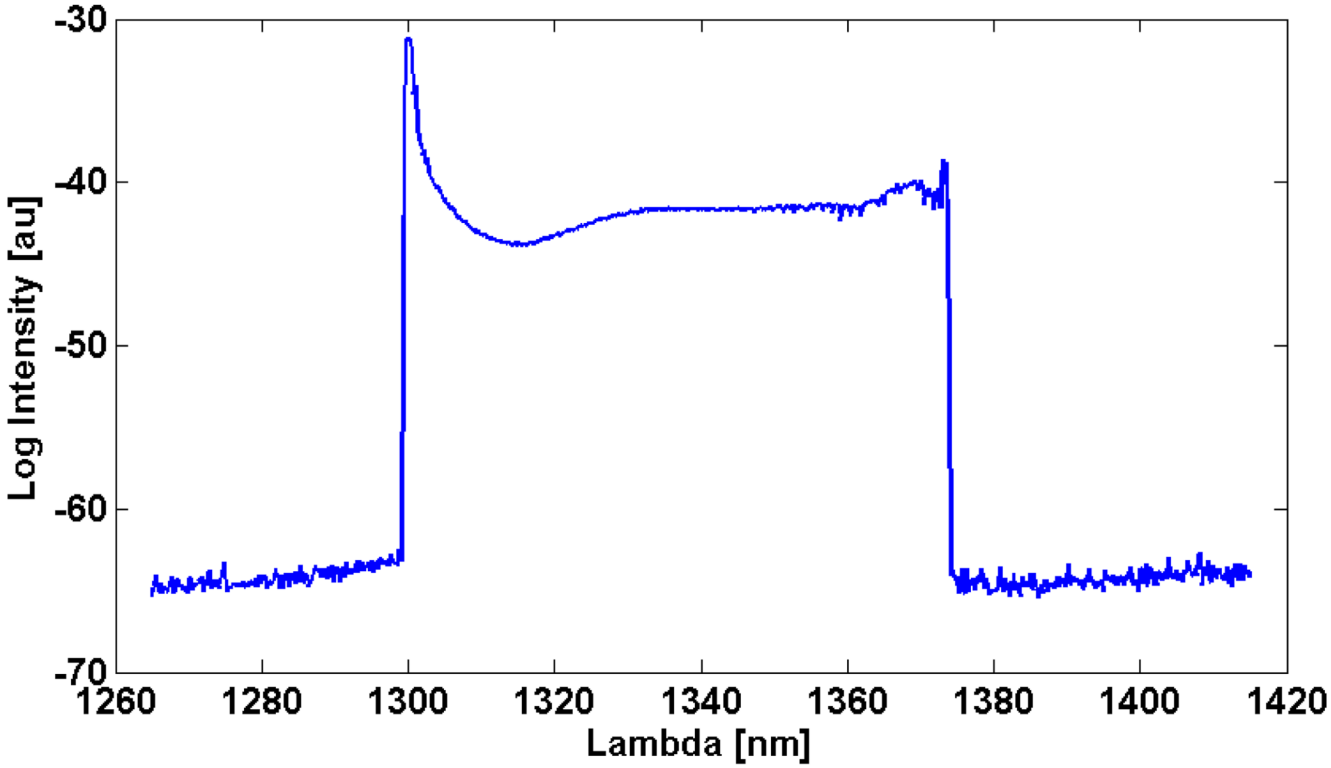

Fig. 4.

Tuning bandwidth, shown in log scale. The peaks at the edges are a sampling artifact as a result of the sinusoidal non-linear drive of the resonant scanner resulting in increased time spent at the edges.

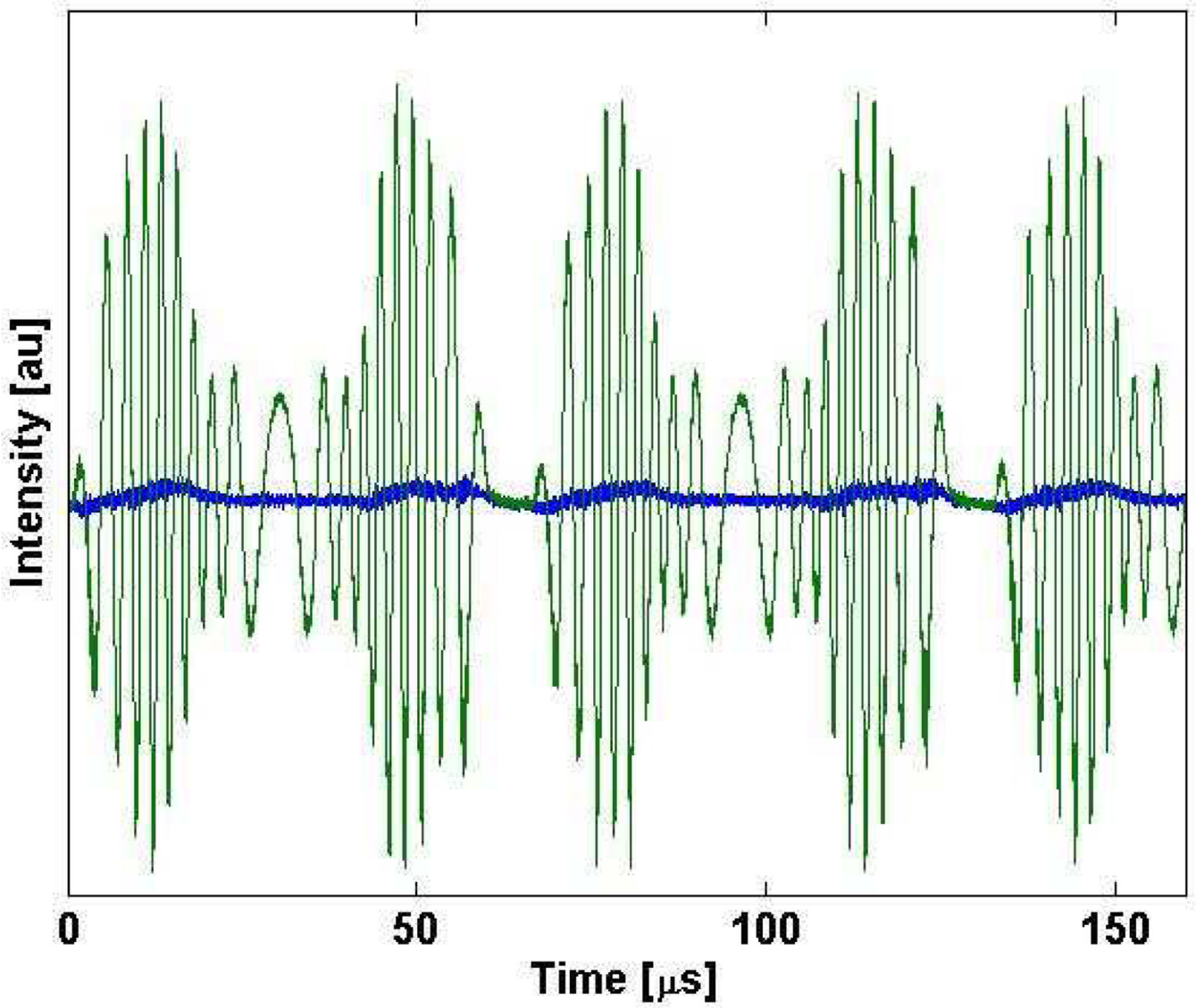

Fig. 5.
Characteristic fringe pattern (green) from a fixed reflector. Dual-balanced reference trace is shown in blue.

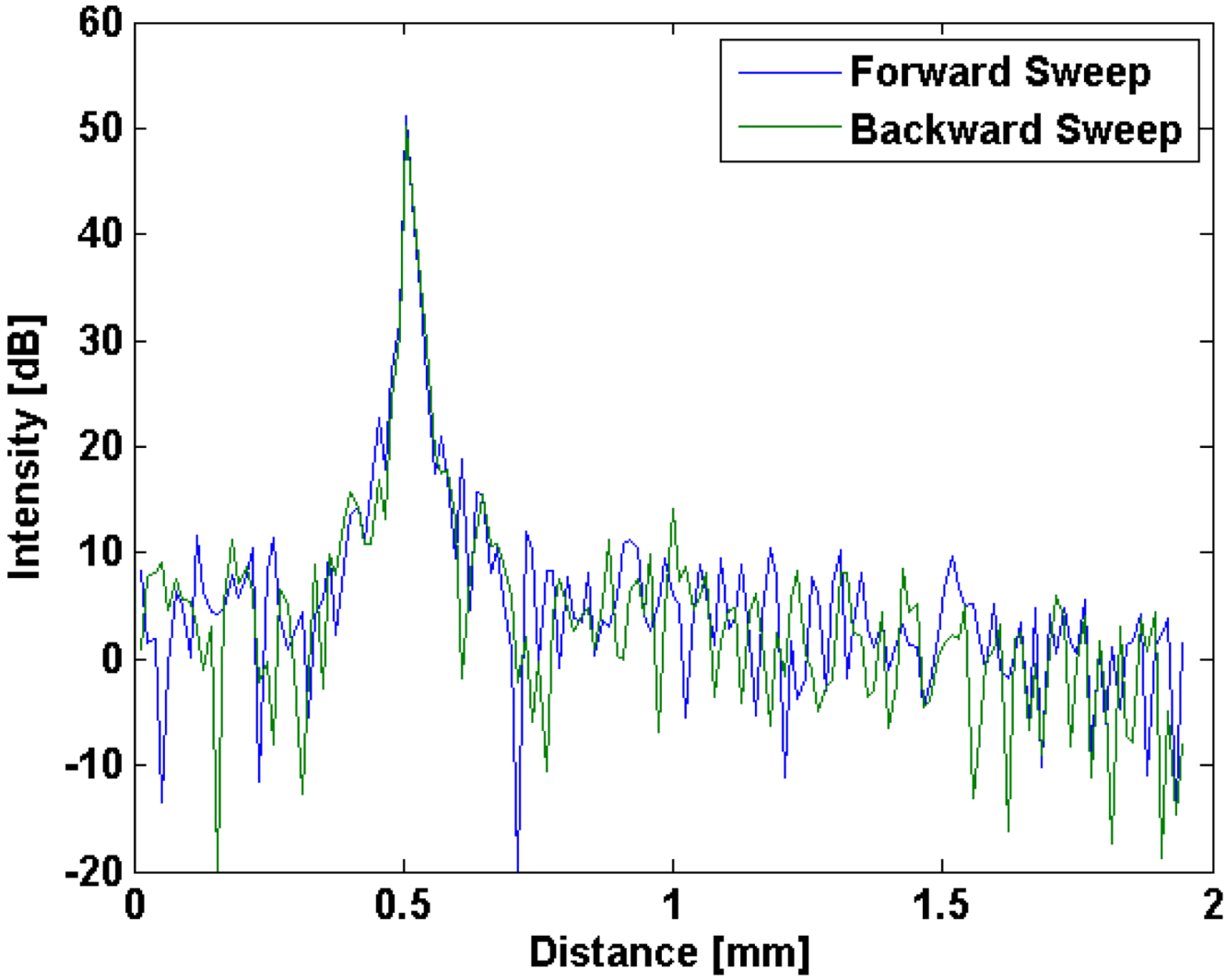

Fig. 6.

Axial point-spread function from a fixed reflector at 500 μm taken with a 43.5 dB attenuator in the sample arm. The forward sweep (blue) and backward sweep (green) are nearly identical in both SNR and axial resolution.

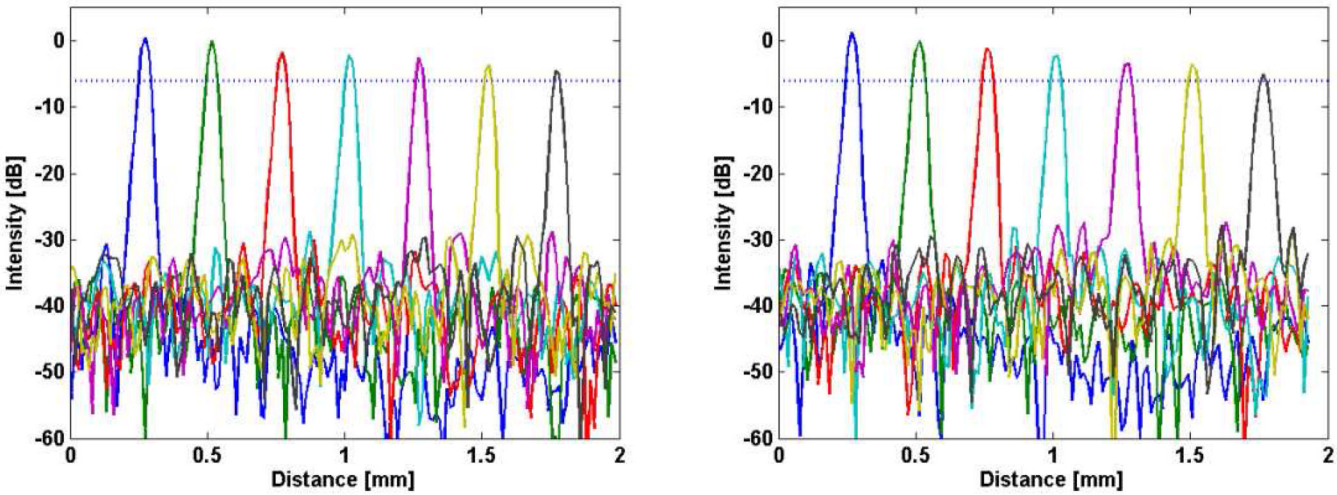

Fig. 7.

Signal roll-off as a function of depth for the forward (left) and backward (right) wavelength sweeps. Both sweeps can achieve > 1.75 nm ranging depth as measured by a 6 dB drop off in SNR from that at zero delay.

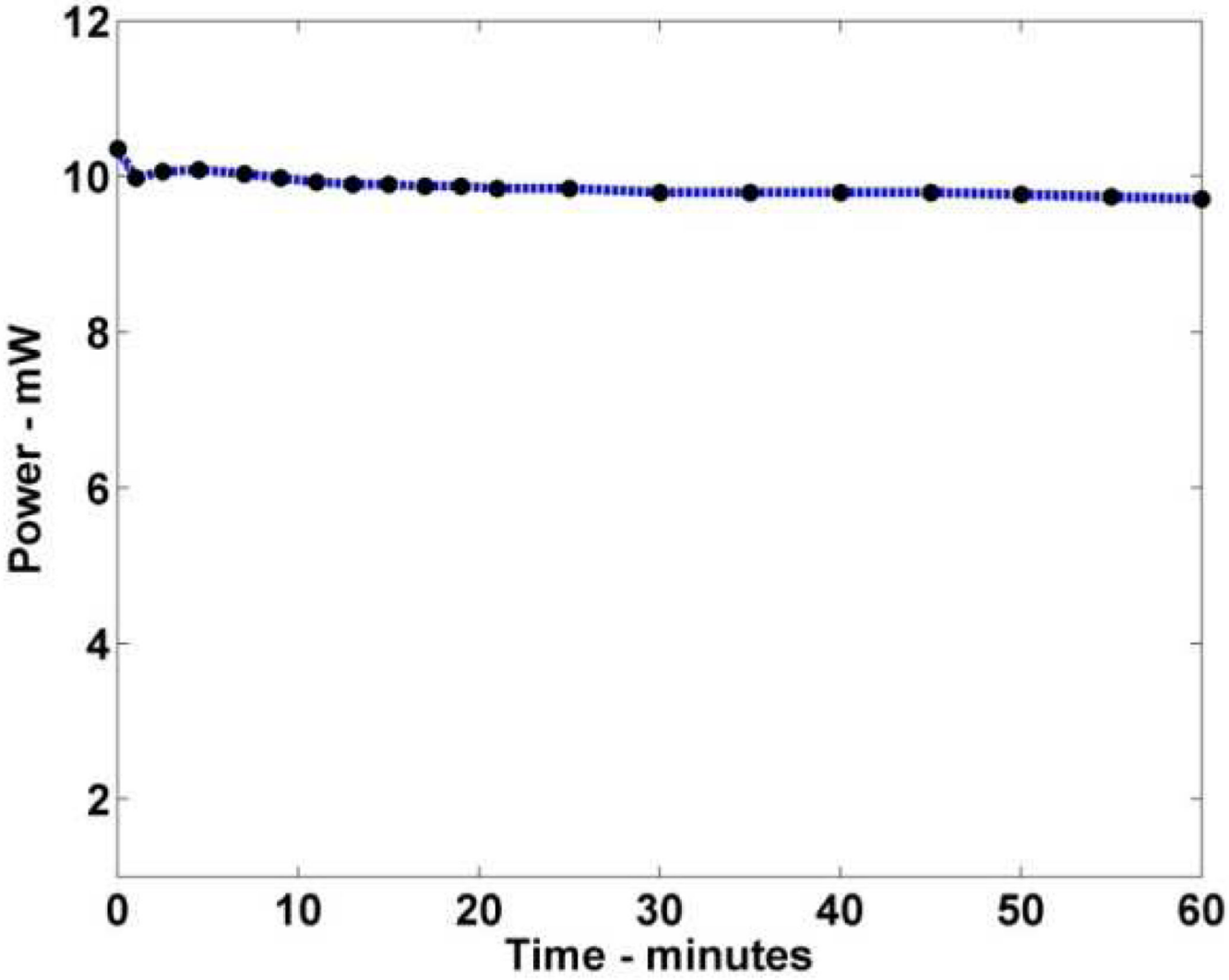

Fig. 8.
Laser output power as a function of time on full battery power. Minimal power loss is observed with over an hour of continuous use.

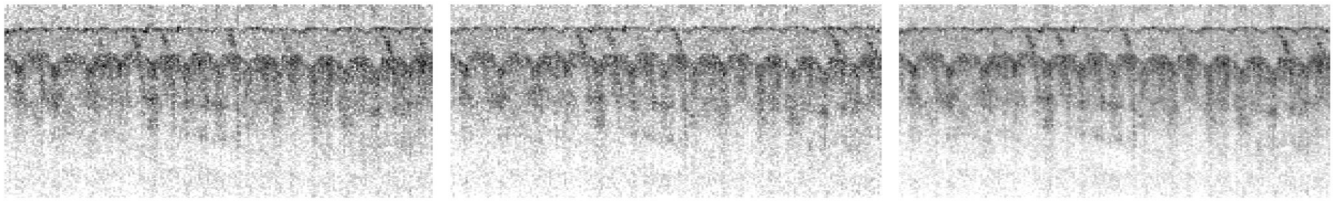

Fig. 9.
5 mm × 2.25 mm OFDI images from the ventral surface of a human forefinger. Forward (left), backward (middle), and combined (right) wavelength sweep images.